Materials Research Express

PAPER • **OPEN ACCESS**

Hierarchical honeycomb metamaterials based on monohedral triangular, square and hexagonal tessellations

To cite this article: Michele Cavaliere and Luke Mizzi 2025 *Mater. Res. Express* **12** 095803

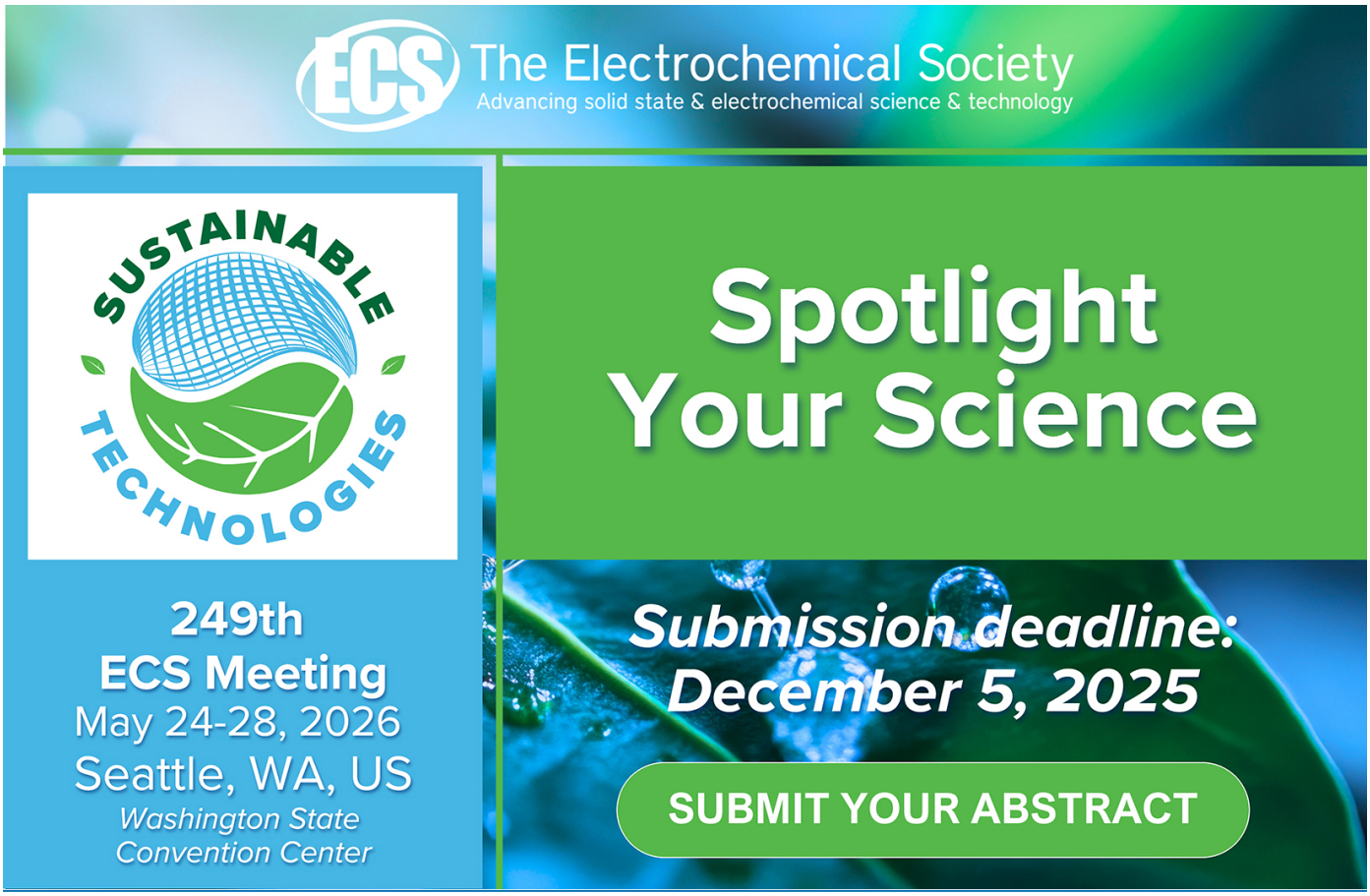

Materials Research Express

OPEN ACCESS

RECEIVED
1 July 2025

REVISED
26 August 2025

ACCEPTED FOR PUBLICATION
5 September 2025

PUBLISHED
15 September 2025

PAPER

Hierarchical honeycomb metamaterials based on monohedral triangular, square and hexagonal tessellations

Michele Cavaliere and Luke Mizzi*

Department of Sciences and Methods for Engineering, University of Modena and Reggio Emilia, Reggio Emilia, Italy

* Author to whom any correspondence should be addressed.

E-mail: luke.mizzi@unimore.it

Keywords: auxetic metamaterials, zero Poisson"s ratio, honeycomb systems, hierarchical structures, tessellations

Abstract

Hierarchical mechanical metamaterials are a class of architectured materials characterised by structures within structures. In this work we present a new class of honeycomb-based hierarchical metamaterials which incorporate irregular honeycombs within the three class of regular monohedral 2D tessellations; namely the triangle, square and hexagonal tessellations. The introduction of hierarchy within these frameworks imparts a high level of versatility in terms of permissible mechanical properties, including anomalous properties such as auxeticity and zero Poisson's ratio, which are not found in the original tessellations. Furthermore, by preserving the original symmetry characteristics of the base tessellations, other advantageous properties, such as transverse isotropy in the case of the triangular and hexagonal tessellations, are retained as well. A wide range of systems were analysed using Finite Element simulations, followed by experimental tests on three additively-manufactured prototypes; one representative architecture of each hierarchical tessellation. The findings of this study demonstrate the transformative effect which the introduction of hierarchy can have on the mechanical properties and deformation behaviour of even the most basic of tessellations as well as opening up new avenues for further studies on the development of novel mechanical metamaterials.

1. Introduction

Mechanical metamaterials represent a class of structured-materials which exhibit unusual and counterintuitive mechanical properties primarily as a result of their architecture, rather than chemical composition. These anomalous characteristics include negative properties such as a negative Poisson's ratio (also known as auxeticity [1–3]). Unlike conventional materials, which tend to contract transversely when subjected to tensile loading, auxetic metamaterials exhibit a negative Poisson's ratio, meaning that they expand in the direction perpendicular to the applied force. This unique property makes them suitable for a wide breadth of applications, ranging from biomedical implants such as stents [4–7], to the design of protective personal equipment and shock absorbers [8, 9].

Auxetic materials possess intricate geometries designed to deform in specific ways, which give rise to their unique and distinctive properties. These systems are classified into four main groups: re-entrant structures [10–13], rotating unit systems [14, 15], chiral honeycombs [16–19] and origami folds [20, 21] and each class comprises systems with various symmetry forms and typologies. Beyond this range of structures, hierarchical auxetic metamaterials [22–24], which incorporate multiple geometries in a single system, have also been introduced to further enhance the mechanical properties of these architectures. Hierarchical metamaterials can either be fractal-based [25–27], i.e. they are designed recursively, creating self-similar structures based on a single geometric feature, or they can be formed through multiple types of geometries combined together at different scales [28–36]. The introduction of hierarchy has been demonstrated to be capable of enhancing properties such as strength-to-weight ratio, influence fracture modes and also conferring increased geometric

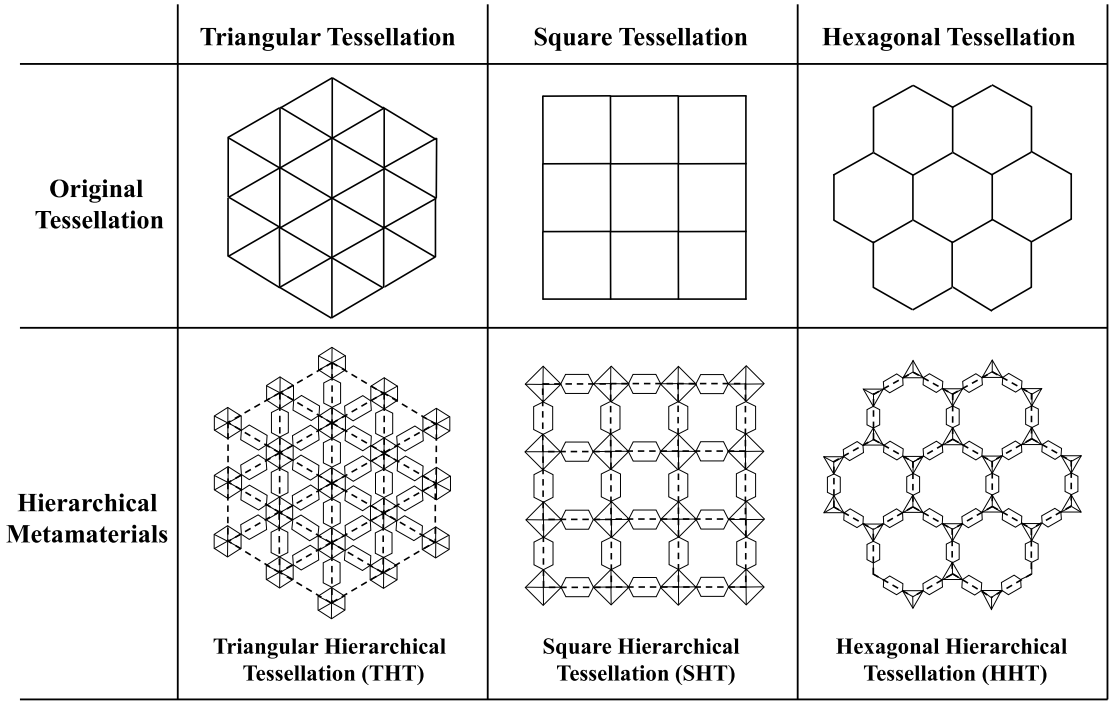

Figure 1. Schematic showing how the hierarchical architectures are formed from the original monohedral tessellations.

versatility resulting in a wider range of permissible mechanical properties (including more negative Poisson's ratios) in comparison to non-hierarchical systems. In fact, previous studies in this have shown that implementing higher-order hierarchies can in some cases, impart auxeticity in non-auxetic tessellations [37]. In auxetic single-level systems, the introduction of hierarchy has also been shown to have the potential to result in more negative Poisson's ratios [22, 33, 38]. Furthermore, hierarchy can also be used to retain the auxeticity of certain systems while improving considerably other mechanical properties such as strain tolerance, energy absorption characteristics and stiffness-density ratios [27, 29, 30].

In this work, we aim to exploit the advantages of hierarchical designs to propose a new class of honeycomb-based metamaterials based on monohedral, regular triangular, square and hexagonal tessellations (see figure 1). These original space-filling tessellations are typically characterised by a positive Poisson's ratio, however, once transformed through the introduction of hierarchical hexagonal linkers, the mechanical properties of these systems change drastically, with some forms even exhibiting auxetic behaviour. Through the use of numerical simulations and experimental tests on 3D-printed prototypes, we demonstrate the vast range of mechanical properties which these systems are capable of possessing and how one may tailor these characteristics as a function of geometric parameters.

2. Description of hierarchical structures

The hierarchical architectures were designed using the only three forms of 2D monohedral tessellations formed from regular polygons, namely triangles, squares and hexagons and are hereby denoted as Triangular Hierarchical Tessellation (THT), Square Hierarchical Tessellation (SHT) and Hexagonal Hierarchical Tessellation (HHT), respectively. As shown in figure 1, the hierarchical order was implemented by introducing full polygons with a triangular-truss reinforcement at the vertices of the original tessellation which are connected together through hexagonal units. The shapes of the polygons used depend on the number of connections at each vertex, with the THT structure having a hexagon, the SHT system a square polygon and the HHT architecture a triangle. These regular polygons are defined by a single parameter, the length p (see figure 2). On the other hand, the hexagons bridging these polygons are irregular and may be described by three independent parameters: (i) the length of honeycomb parallel to the original tessellation line, h, (ii) the length of the other four ligaments, l and (iii) the aperture angle between ribs of these two lengths, θ. The final parameter is the thickness of the ligaments, t, which was kept constant throughout for all tessellations.

The introduction of hierarchy does not alter the symmetric framework of the original tessellations and, thus, these systems retain their original symmetry and periodic characteristics. This means that each system can be studied through a single representative unit cell with an identical aspect ratio to the original tessellation.

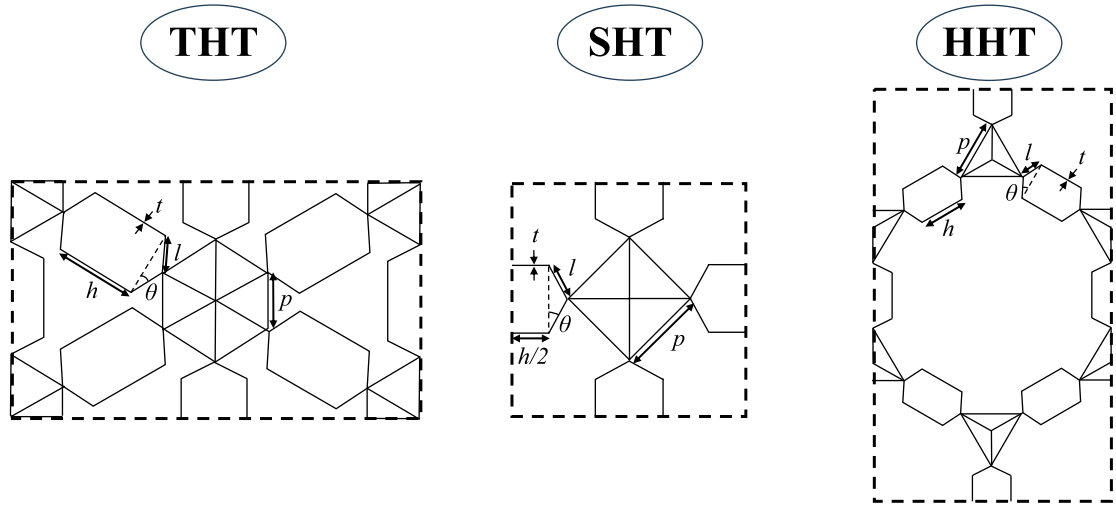

Figure 2. Illustration of the representative unit cell of each hierarchical tessellation studied and the independent geometric parameters used to define these systems.

These representative unit cells are illustrated in figure 2 below. Given that both the THT and HHT systems are characterised by in-plane hexagonal symmetry, these architectures must be transversely-isotropic [39, 40] and therefore the mechanical properties of the system remain unchanged regardless of the chosen orientation of the unit cell. The SHT system, on the other hand, is expected to exhibit identical mechanical properties at 90° rotational intervals by virtue of its square symmetry, similar to the original square tessellation.

At this point, it is worth mentioning that for each tessellation, there are some geometric construction constraints which must be respected in order for the architectures to realisable without overlap of the ligaments making up the system. These conditions, which are different for each system, may be defined as follows:

$$\text{THT } l\cos\left(\theta+\frac{\pi}{6}\right)<\frac{p}{2} \tag{1}$$

$$\text{SHT } l\cos\left(\theta+\frac{\pi}{4}\right)<\frac{p}{2} \tag{2}$$

$$\text{HHT } l\cos\left(\theta+\frac{\pi}{3}\right)<\frac{p}{2} \tag{3}$$

3. Methodology

In order to study the influence of hierarchical geometries on metamaterials, a numerical and an experimental approach were used. First, a wide-ranging parametric analysis involving a large number of configurations for each type of hierarchical tessellation was conducted using Finite Element (FE) simulations for small-strain deformation under periodic boundary conditions. This was then followed by experimental tests on a number of 3D-printed prototypes in order to analyse the deformation behaviour of these systems and validate the results obtained from the initial parametric run.

3.1. Parametric analysis using linear FE simulations

The simulations were carried out using ANSYS16 Multiphysics FE software utilising periodic boundary conditions. The representative unit cell of each system was constructed and meshed using beam elements through the BEAM189 element formulation. This element type is a three-node 3D element with six degrees of freedom and permits large deflection. Three of these degrees of freedom pertain to displacements in the x, y and z directions, while the remaining three concern rotations around the x, y and z axes. A rectangular cross-section was specified for the beam elements and, following convergence tests, the mesh size was set to $p/60$. The material properties of the isotropic ABS plastic were used as constitutive properties; a Poisson's ratio of 0.3 and Young's modulus of 2 GPa.

In order to ensure that the system remained in-plane throughout deformation, the translation of nodes in the z-direction was prohibited, i.e. $U_z = 0$, which in turn results in the blocking of the out-of-plane rotational degrees of freedom as well (ROT_x and ROT_y). For the implementation of in-plane periodicity, mirror-

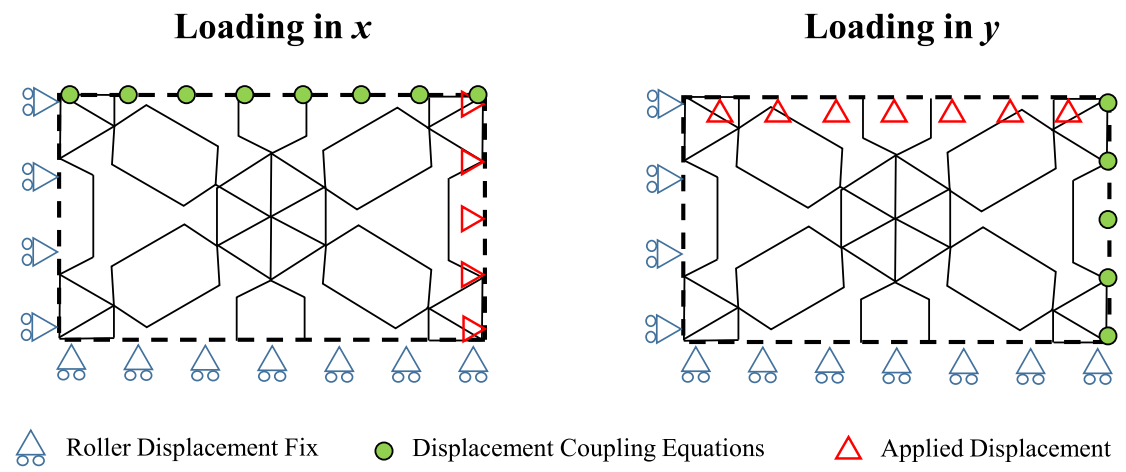

Figure 3. Application of periodic boundary conditions for loading in the *x*- and *y*-directions. Besides the displacement fixes and loads indicated above, coupling equations were also applied pairing all opposing edge nodes for the rotational degrees of freedom according to equation (4).

symmetry-based periodic boundary conditions were used, taking advantage of the presence of the two axes of symmetry in the representative unit cell of each simulated system as shown in figure 3. A roller displacement fix blocking displacement in the *x*-direction ($U_x = 0$) was applied on the nodes on the leftmost edge of the system, while the bottommost edge nodes were blocked in an analogous manner in the *y*-direction ($U_y = 0$). In order to ensure that the nodes in the uppermost and rightmost edges of the cell remain aligned with the *x*- and *y*-axes respectively throughout deformation, coupling equations were used to constrain these nodes to maintain identical displacement values (U_y is constant for all uppermost nodes and U_x is constant for all rightmost nodes). Finally, the in-plane rotational degrees of freedom (ROT_z) of all opposing edge nodes were paired together through the use of coupling equations, where each node on the leftmost and bottommost edges (1) was paired with its corresponding node (n) in the rightmost and uppermost edges (2) respectively through equation (4). This ensures that the rotational deformation is also periodic.

$$ROT_z(n_1) - ROT_z(n_2) = 0 \tag{4}$$

In order to obtain the mechanical properties, the systems were subjected to uniaxial loading in the *x*- and *y*-directions separately. Loading was applied through the imposition of a small displacement on the uppermost nodes in the *y*-direction for *y*-loading and a small displacement in the rightmost nodes in the *x*-direction for loading in this direction. A linear solver was used to run the simulation and the Poisson's ratio was extracted by measuring the strains in the axial and transverse directions, while the Young's modulus was calculated after extracting the reaction forces from the edge nodes upon which the displacement was imposed. Further details on the theory behind the simulation methodology used and extraction of results can be found in [41, 42].

In order to carry out the parametric simulation run, a large number of configurations were analysed within the limits of the geometric constraints specified in equations (1)–(3). The parameters of the different systems were varied as follows: l was set in a range from 0.5 mm to 10 mm in 0.5 mm increments, h was varied from 0.5 mm to 10 mm in 0.5 mm increments and θ was varied from 5° to 85° in 5° increments. The parameters p and t were kept constant at 5 mm and 0.1 mm respectively throughout, while the out-of-plane thickness was imposed at a unitary value. Therefore, in relative terms, the variables varied were l/p from 0.2 to 2 and h/p from 0.2 to 2. These combinations generated over 4000 configurations for each of the three hierarchical systems, although a few systems did not satisfying the geometric constraints making certain combinations of variables inadmissible since they result in unrealizable configurations.

3.2. Experimental tests on additively manufactured prototypes

The parametric analysis was then followed by experimental tests on a number of 3D-printed prototypes in order to analyse the behaviour of these systems at small strains and validate the results obtained from the initial simulation run. One architecture representative of each hierarchical tessellation was fabricated using a Bambu Lab® X1 Carbon Fused-Deposition Method (FDM) 3D-Printer in ABS using 100% rectilinear infill with two wall loops and no supports. The dimensions and relative parameters of these systems were chosen on the basis of the results obtained from the parametric study described in the previous section and the design constraints imposed by the 3D-printer resolution and platform space. For ease of comparison of the three systems, we selected configurations which have identical ligament thicknesses and a similar global resultant size (gauge

Table 1. Parameters of 3D-printed prototypes. L_x and L_y represent the gauge lengths of the global systems.

Structure 1 (THT)									
p (mm)	l (mm)	h (mm)	θ (°)	t (mm)	d (mm)	L_x (mm)	L_y (mm)	RUC_x	RUC_y
16.5	9.9	3.3	15	1	20	215.25	207.12	3	5
Structure 2 (SHT)									
9	18	9	35	1	20	211.88	211.88	5	5
Structure 3 (HHT)									
15	15	3	5	1	20	198.62	206.42	5	3

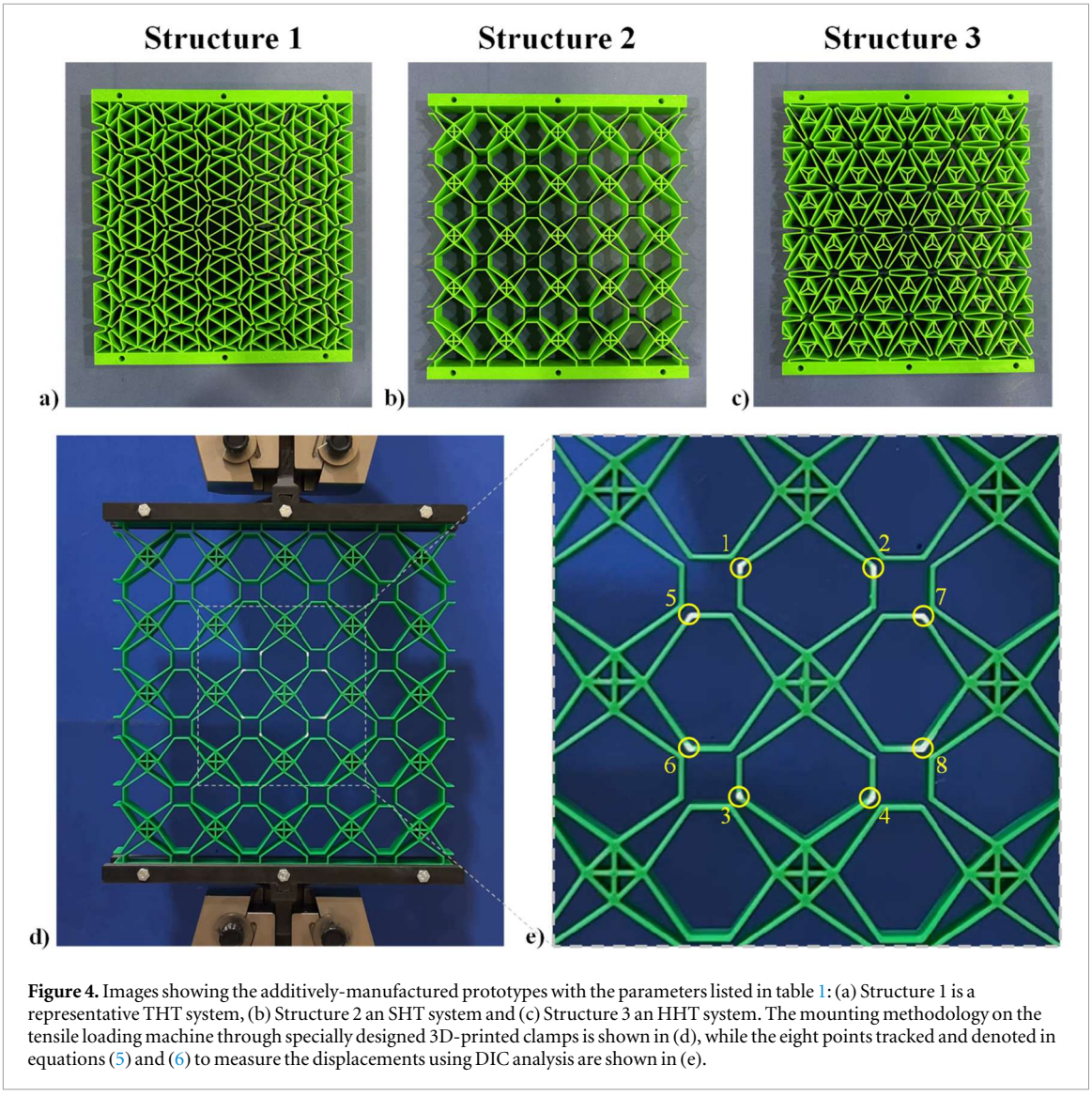

Figure 4. Images showing the additively-manufactured prototypes with the parameters listed in table 1: (a) Structure 1 is a representative THT system, (b) Structure 2 an SHT system and (c) Structure 3 an HHT system. The mounting methodology on the tensile loading machine through specially designed 3D-printed clamps is shown in (d), while the eight points tracked and denoted in equations (5) and (6) to measure the displacements using DIC analysis are shown in (e).

length). The two systems representative of the THT and HHT systems, hereby denoted as Structures 1 and Structure 3, were designed with 3×5 and 5×3 representative unit cells, while the SHT system (Structure 2) was design as a 5×5 system. All three structures were designed with an in-plane ligament thickness, t, of 1 mm and an overall out-of- plane thickness, d, of 20 mm. The full list of parameters are shown in table 1, while images of the additively-manufactured prototypes are provided in figures 4(a)–(c).

In order to analyse the mechanical properties of these systems, the structures were subjected to uniaxial tensile loading using a Galdabini® tensile loading machine with a 2500 N loadcell. Custom-clamps (designed and 3D-printed specifically for this purpose) were used to attach the upper and lower part of the prototypes to the loading machine as shown in figure 4(d). The systems were subjected to a tensile displacement of 20 mm

each, equivalent to *ca*. 10% global strain, at a rate of 5 mm min^{-1}. The tensile loading test was recorded with a camera and a Digital Imaging Correlation (DIC) analysis was carried out to measure the Poisson's ratio. As shown in figure 4(e), (a) number of points were marked with white paint on the central representative unit cell of each architecture. These points were tracked using a Matlab® subroutine throughout deformation [43] and their relative displacements were used to measure the average strains as follows:

$$\bar{\varepsilon}_x = \frac{1}{2}\left(\frac{(X5_i - X7_i) - (X5_0 - X7_0)}{X5_0 - X7_0} + \frac{(X6_i - X8_i) - (X6_0 - X8_0)}{X6_0 - X8_0}\right) \tag{5}$$

$$\bar{\varepsilon}_y = \frac{1}{2}\left(\frac{(Y1_i - Y3_i) - (Y1_0 - Y3_0)}{Y1_0 - Y3_0} + \frac{(Y2_i - Y4_i) - (Y2_0 - Y4_0)}{Y2_0 - Y4_0}\right) \tag{6}$$

where Xn_0 and Yn_0 represent the x- and y-coordinates of the point n in the first reference image respectively and Xn_i and Yn_i represent the x- and y-coordinates of the same point n in the subsequent images. The engineering Poisson's ratio was then measured for each image using:

$$\nu = -\frac{\bar{\varepsilon}_x}{\bar{\varepsilon}_y} \tag{7}$$

In addition to these experimental tests, corresponding nonlinear geometric simulations were carried out on periodic equivalents of these prototypes with large deflections allowed over an 8% tensile strain range. These simulations allowed for a comparison between the experimental and simulated systems whilst accounting for geometric nonlinearities which may arise during high-strain loading.

4. Results and discussion

In this section, the results obtained from the FE simulations and experimental results are presented in terms of Poisson's ratios, ν, and the Young's effective modulus, E^*. The latter is a unitless value obtained by dividing the metamaterial Young's modulus with the constitutive material Young's modulus ($E^* = E_{metamaterial}/E_{material}$) which is used to obtain a relative stiffness value that is characteristic of the metamaterial geometry itself, independent of the material utilised. First, the results obtained from the parametric study using linear FE simulations for the analysis of the three tessellations are presented. The values obtained for loading in the x- and y-directions were identical, as expected, since the symmetry characteristics of these metamaterials impart in-plane isotropic behaviour in the case of the THT and HHT systems and identical mechanical properties at 90° rotational intervals in the case of the SHT system, and thus the results obtained can be represented by a single Poisson's ratio and Young's effective modulus value. It is worth noting that although the small strain mechanical properties presented in this section were obtained from tensile loading, they also apply for small strain compressive loading. Following the analysis of the FE results, the findings of the experimental tests are discussed.

4.1. Triangular hierarchical tessellation (ThT)

A representative data set for the THT structures comprising of structures with an h/p ratios of 0.2, 0.6 and 1.0 and varying θ and l/p variables is presented in figure 5. The trends observed for these systems where similar to those obtained for the remaining simulated structures and were chosen on the basis that they provide an encompassing view of the general influence which the geometric parameters have on the mechanical properties of these hierarchical systems.

It is evident from the plots in figure 5, that the Poisson's ratio varies considerably as θ and l/p vary, from a range of +0.5 to −0.15. The highest Poisson's ratio were consistently obtained for systems with a large θ value and a low l/p value. On the other hand, the lowest values were obtained for configurations with a relatively large l/p dimension and a small θ angle. While for systems, with large h/p values (i.e. $h/p > 0.3$) the lowest values where in the range of +0.3 to 0, for systems with lower h/p values, auxetic structures with a low magnitude negative Poisson's ratio may be obtained, with the lowest value being –0.15 for the system shown in figure 6(a) with the parameters: $h/p = 0.2$, $l/p = 0.6$ and $\theta = 5°$. In terms of effective Young's modulus, relatively low values were obtained for almost all the simulated systems, with orders of magnitude varying between 1×10^{-4} and 1×10^{-6}. The highest values were obtained for configurations with large θ and low l/p ratios, with the maximum E^* value being 2.13×10^{-4} for the structure shown in figure 6(b), which has $h/p = 1.0$, $l/p = 0.4$ and $\theta = 60°$.

In figure 6, a magnified illustration of the deformation observed in the two aforementioned specific cases upon loading is presented. In figure 6(a), the system which exhibits a negative Poisson's ratio is shown being loaded in the x-direction. It is evident that the auxeticity arises as a result of the hexagonal honeycombs opening up resulting in widening in both axial and transverse directions. This deformation mechanism is particularly

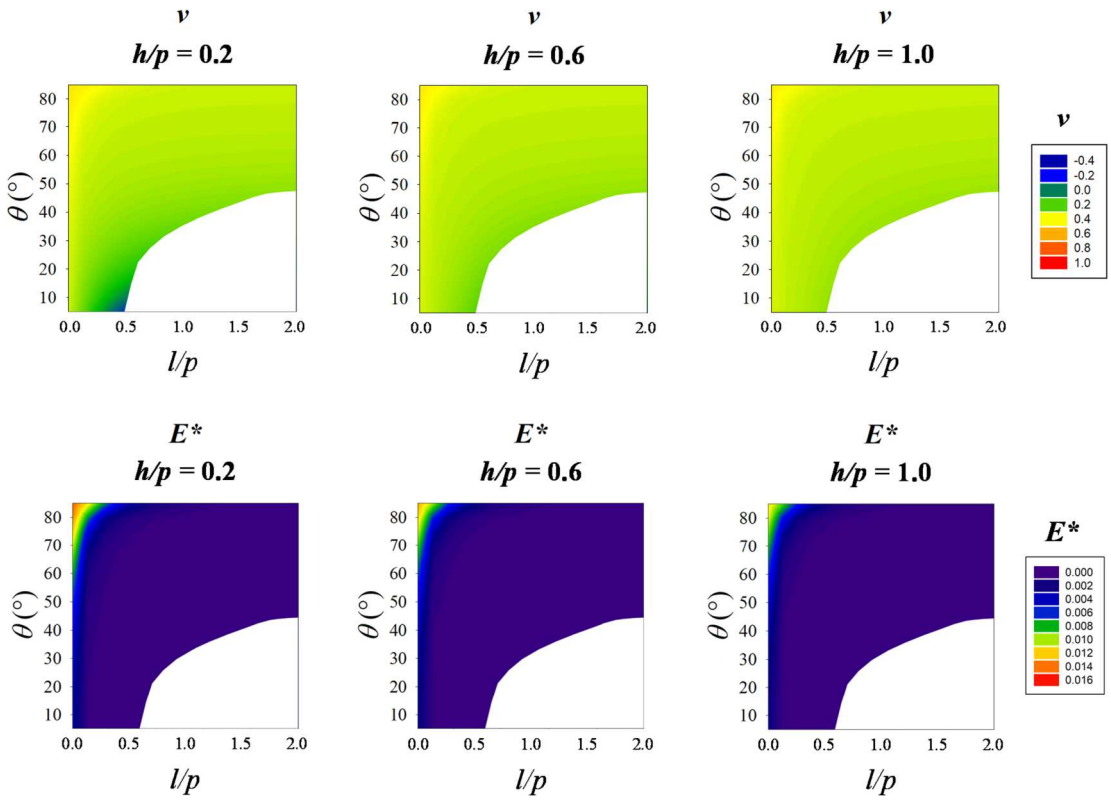

Figure 5. Plots showing how the Poisson's ratios and effective Young's moduli vary for the THT systems upon changing θ and l/p for various h/p values. The minimum Poisson's ratio was obtained from the $h/p = 0.2$ set at -0.15, while the highest value of for $h/p = 1.0$ set at $+0.5$. In the case of E^*, the minimum value obtained was 1.39×10^{-6} while the maximum value was 0.014. The white area denotes the region of unrealisable geometries which do not satisfy the criterion in equation (1).

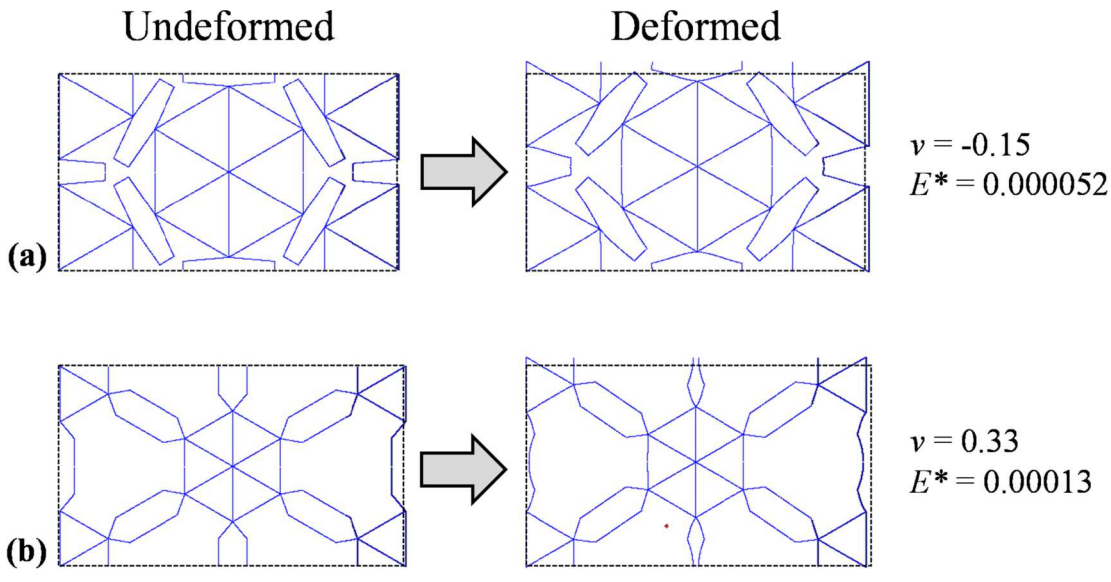

Figure 6. Images showing the undeformed and magnified deformed states of two representative THT systems upon uniaxial tensile loading in the y-direction. The geometric parameters of these systems are defined as follows: (a) $h/p = 0.2$, $l/p = 0.6$ and $\theta = 5°$ and (b) $h/p = 1.0$, $l/p = 0.4$ and $\theta = 50°$.

favoured in honeycomb systems with an l/p dimension which is much larger relative to h/p and very small θ angles and it is these configurations (which are extremely close to the geometric realizability limitation indicated in equation (1)), which have the capability of exhibiting auxetic behaviour. The second example, shown in figure 6(b), pertains to a system which exhibits a highly positive Poisson's ratio and a relatively high effective Young's modulus. It is clearly shown that in this case the deformation mechanism is completely different, with

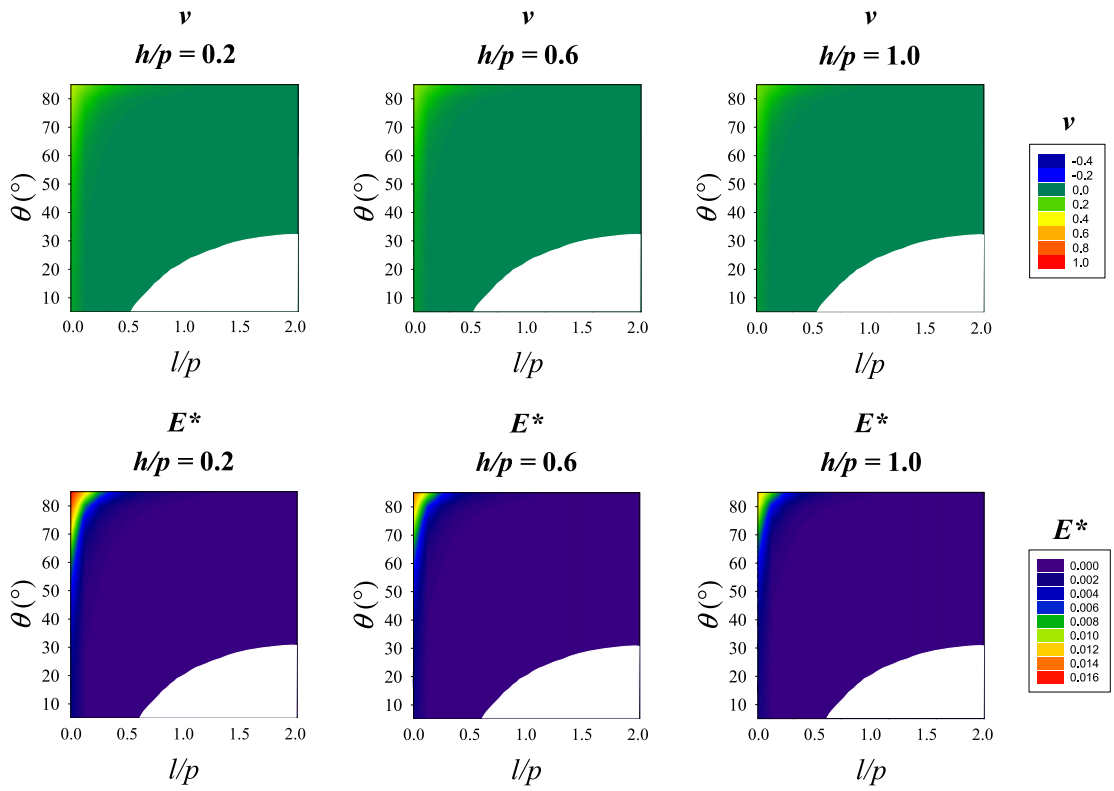

Figure 7. Plots showing how the Poisson's ratios and effective Young's moduli vary for the SHT systems upon changing θ and l/p for various h/p ratios. The Poisson's ratio was roughly zero for nearly all configurations. In the case of E^*, the minimum value obtained was 9.31×10^{-7} while the maximum value was 0.016. The white area denotes the region of unrealisable geometries which do not satisfy the criterion in equation (2).

the ligaments of length h deforming significantly more than those of length l. This localised hexagonal honeycomb deformation mode is analogous to that of a stretching non-hierarchical hexagonal honeycomb system and previous studies found in the literature on these systems have shown that honeycombs with small l/h ratios and large θ values also exhibit very high stiffness values and non-auxetic behaviour as in the case here [10, 44].

4.2. Square hierarchical tessellation (Sht)

For the SHT system, on the other hand, it is evident that almost all configurations exhibit a Poisson ratio of almost zero, except for an extremely small subset of structures with very small h/p and l/p ratios coupled with a very large θ value which show a positive Poisson's ratio (see figure 7).

As shown in figure 8(a), where a representative zero Poisson's ratio system with the parameters $h/p = 1.0$, $l/p = 2.0$, $\theta = 35°$ is shown, this behaviour arises from the fact that for loading in the x-direction, only the hexagonal cells aligned along this direction elongate, while the other, vertically-aligned set, remain undeformed. The opposite is true for loading in the y-direction; in this case only the vertically-oriented honeycomb cells deform whilst the others remain undeformed. In both cases, this deformation mechanism results in an elongation of the system in the loading direction only, whilst the transverse direction remains unchanged.

Since the deformation occurs almost entirely through the irregular hexagons, then it stands to reason that the effective global stiffness of these systems is also determined by the geometric parameters of the hexagons. For these systems, the E^* values obtained range over three orders of magnitude, with the highest value obtained being 0.016. This variation can be entirely explained in terms of hexagonal honeycomb mechanical considerations [10, 44], with systems possessing hexagons with small h/p and l/p ratios and large θ values (i.e. the honeycombs are close to their fully-opened configuration); see figure 8(b), being the most rigid, while systems with large l/h ratios and small θ values being the most pliant and deformable. This also explains why some systems which represent extreme variations of the irregular hexagon exhibit a positive Poisson's ratio. In these systems, which conform to the former case, the hexagonal honeycomb is so stiff, that the deformation is extended also to the central square-truss unit resulting a contraction in the lateral direction upon stretching in the axial direction. This hypothesis is also supported by the fact that these structures also represent the stiffest configurations of the SHT systems.

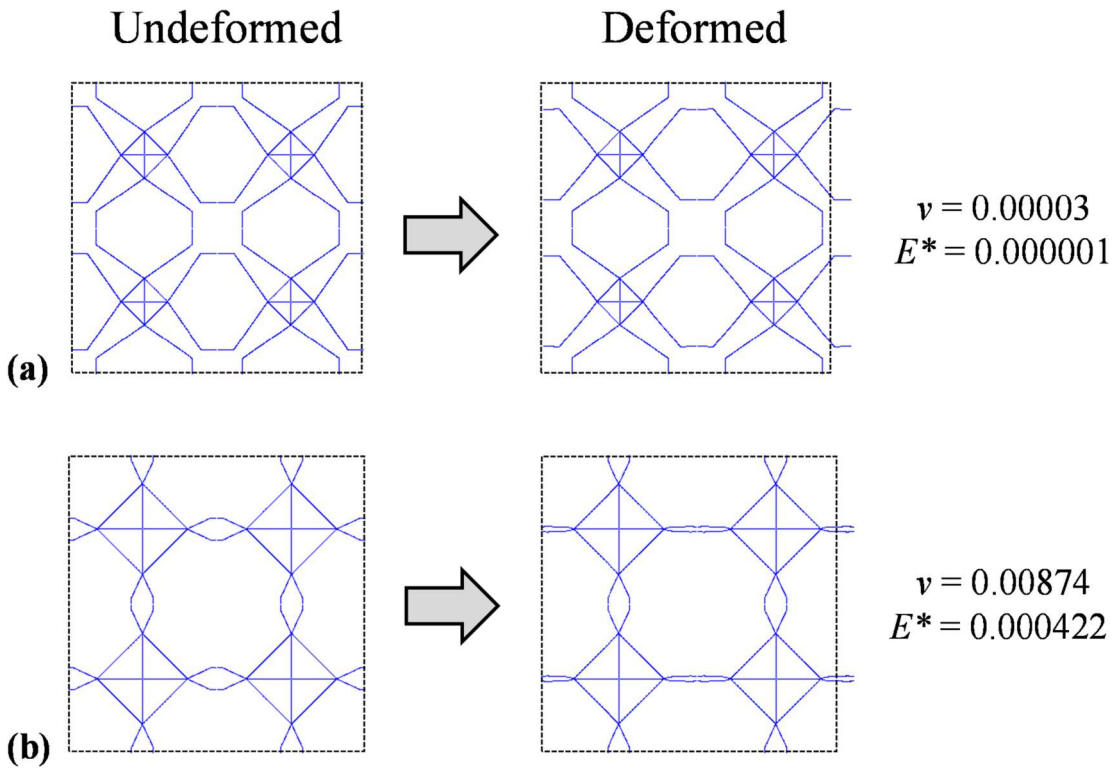

Figure 8. Images showing the undeformed and magnified deformed states of two representative SHT systems upon uniaxial tensile loading in the x-direction. The geometric parameters of these systems are defined as follows: (a) $h/p = 1.0$, $l/p = 2.0$ and $\theta = 35°$ and (b) $h/p = 0.2$, $l/p = 0.4$ and $\theta = 65°$.

4.3. Hexagonal hierarchical tessellation (HhT)

The plots in figure 9 show that for the HHT system is the hierarchical configuration which exhibits the most versatility in terms of mechanical properties. While the majority of simulated structures have a very high Poisson's ratio, in many cases approaching a value of +1, several structures also show negative ν values (up to −0.24) which were unattainable from the THT and SHT systems. Similar to THT systems, the most negative values were obtained for configurations possessing a small θ value coupled with large l/p ratios and small h/p ratios.

An example of a negative Poisson's ratio architecture is shown in figure 10(a) for the system with $h/p = 0.2$, $l/p = 1.1$ and $\theta = 5°$. It is clear, that upon loading in the x-direction, all the irregular hexagons deform to varying extents, resulting in both an axial and lateral expansion. In mechanical terms, this deformation mechanism can be likened to the global stretching-based deformation mechanism described by Masters and Evans [10] of non-hierarchical conventional regular hexagons, with the small hexagons acting as springs which elongate the hexagonal frame in all directions. In the original hexagonal tessellation upon which the HHT architecture is based, the stretching-based mechanism (which is predicted to give rise to auxetic behaviour) is not active, since it is considerably stiffer than flexure which is, therefore, mechanically favoured and more dominant. However, the introduction of hierarchy causes a change of deformation mode with the end result which is similar to that of the stretching model in terms of Poisson's ratio.

This analogy between the different deformation modes of regular hexagonal honeycombs and these hierarchical systems also extends to the systems which show a highly positive Poisson's ratio such as the one shown in figure 10(b). Here, the hexagons bridging the triangular interconnections possess small θ values which means that these hexagons are similar in shape to the simple ligaments found in a non-hierarchical regular honeycomb system. This results in a deformation mode which is also similar to that of the non-hierarchical structures, dominated by hinging or flexure of ligaments [10]. Both of deformation modes result in an extremely large positive Poisson's ratio of +1 such as the one obtained for the hierarchical systems.

These mechanistic considerations also apply to the effective Young's moduli results. From figure 9, it is clear that for this hierarchical tessellation, systems with extremely small θ values and small l/p ratios exhibit the highest level of stiffness. This finding may appear anomalous in comparison to the THT and SHT systems, however it may be explained by interplay between the Level 0 (small triangles and irregular hexagons) and Level 1 (original regular hexagonal tessellation) geometry. Systems with small θ angles and lengths l/p, result in small interconnection distances between triangles (in essence a small, wide honeycomb), hence forming small, 'thick

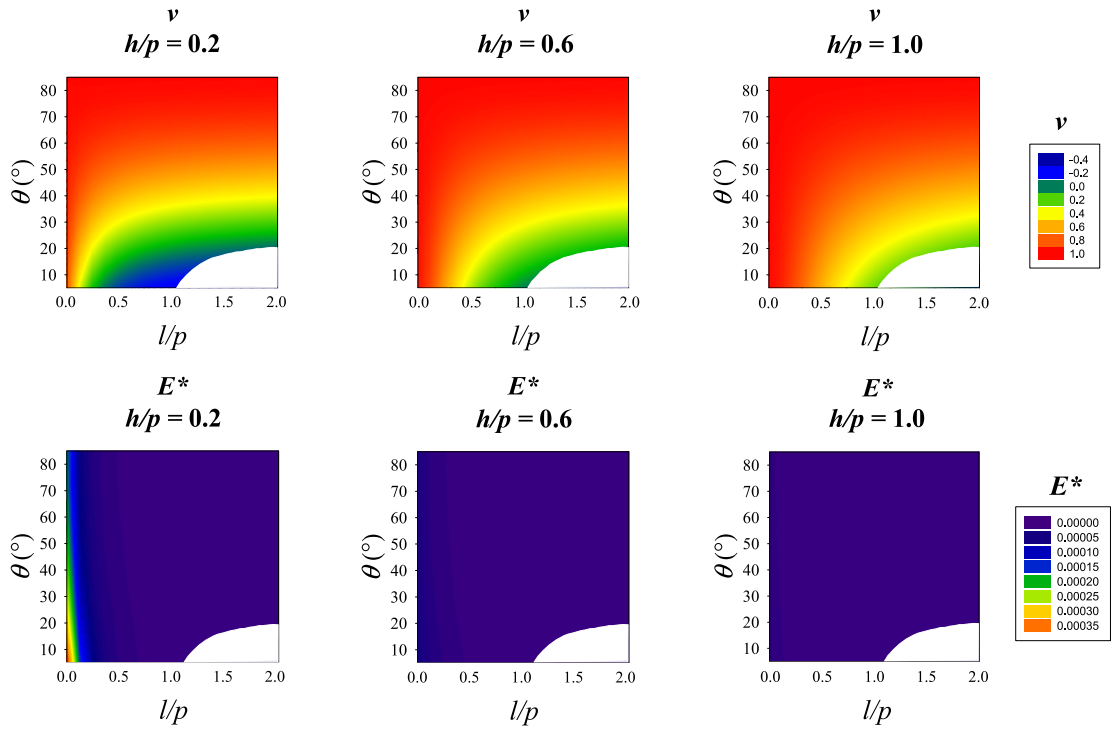

Figure 9. Plots showing how the Poisson's ratios and effective Young's moduli vary for the HHT systems upon changing θ and l/p for various h/p values. The minimum Poisson's ratio was obtained from the $h/p = 0.2$ set at -0.24, while the highest value obtained throughout was at $+0.99$. In the case of E^*, the minimum value obtained was 1.48×10^{-7} while the maximum value was 9.95×10^{-4}. The white area denotes the region of unrealisable geometries which do not satisfy the criterion in equation (3).

ligaments' which result in a stiffer global architecture (see figure 10(a)) and a deformation mode dominated by Level 0 deformations resulting in auxeticity. On the other hand, systems with large θ angles and large l/p values are more similar to non-hierarchical systems with long, 'thin ligaments' and hence the Level 1 deformation mode (i.e. regular non-hierarchical honeycomb) is dominant resulting in a far lower level of stiffness and a highly positive Poisson's ratio.

4.4. Comparative analysis of the three hierarchical tessellations

Following the individual analysis of all three hierarchical tessellation, the logical next step is to carry out a comparative examination of these systems. A representative set ($h/p = 0.2$) for the THT, SHT and HHT systems showing the variation in Poisson's ratio and Young's modulus is presented in figure 11. These systems were chosen on the basis that they showcase the widest range of mechanical properties and deformation behaviour for each hierarchical tessellation.

It is evident that the HHT system is the most versatile in terms of Poisson's ratio, with this property ranging from +1 to –0.24. This range encapsulates the most positive and negative values that may be obtained from these hierarchical systems and exceeds that of the SHT and THT systems. The THT system is also shown to exhibit a fairly variable, albeit more restricted, range of Poisson's ratios with most configurations showing a low positive Poisson's ratio and a small subset exhibiting slightly auxetic behaviour. Finally, the SHT system exhibits a nearly constant on-axis Poisson's ratio of zero for nearly all configurations. Although one may consider this to be a disadvantage, it is also of interest since this means that one may tailor the Young's modulus of the system independently of the Poisson's ratio. Furthermore, zero Poisson's ratio architectures are considered useful and interesting in their own right since they have the potential to exhibit unique properties such as monoclastic curvature [45–47].

In terms of Young's moduli, it is clear that the SHT and THT systems exhibit a superior level of structural stiffness in comparison to the HHT systems, with the THT systems being the stiffest tessellations. In comparison, the HHT systems show a far lower effective Young's modulus range which is at least two orders of magnitude less. This observation is in accordance with the trends noted for the non-hierarchical counterparts of these tessellations; with the tensile deformation of the triangular and square 2D lattice structures being dominated by stretching of ligaments (hence, high stiffness) and the hexagonal lattice being characterised by flexural and bending deformations (thus a lower relative stiffness) [48, 49].

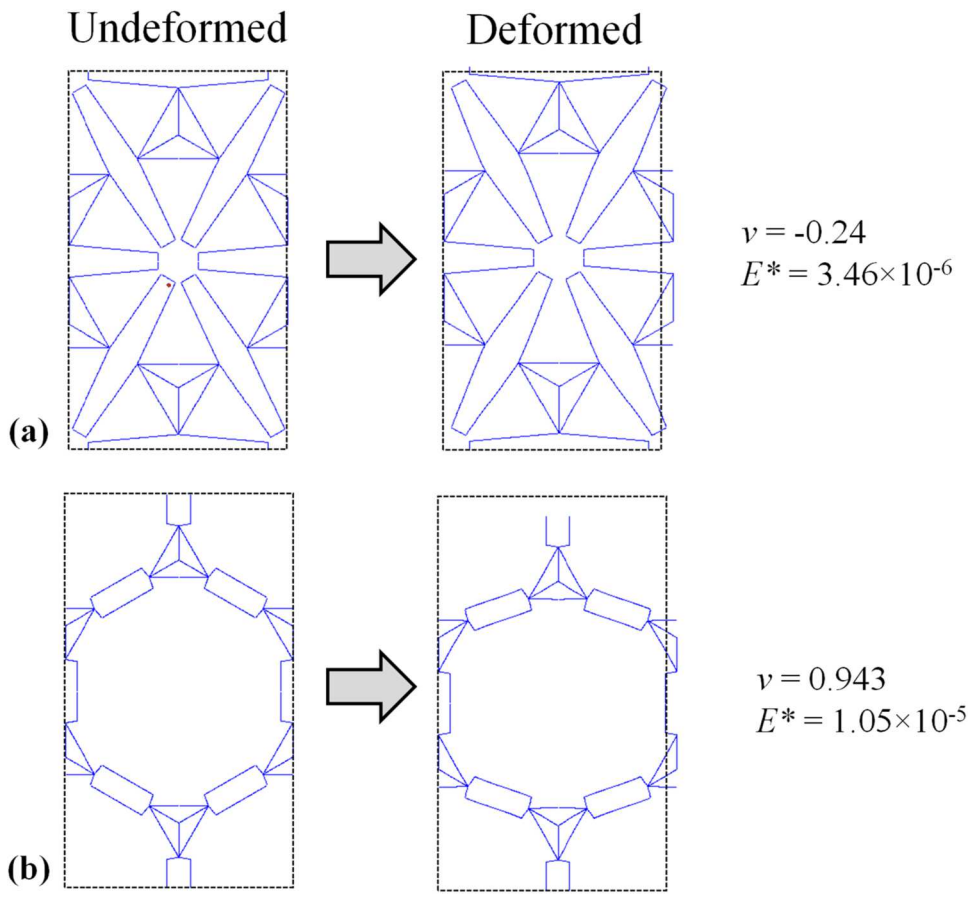

Figure 10. Images showing the undeformed and deformed states of two representative HHT systems upon uniaxial tensile loading in the x-direction. The geometric parameters of these systems are defined as follows: (a) $h/p = 0.2$, $l/p = 1.1$ and $\theta = 5^\circ$ and (b) $h/p = 1.0$, $l/p = 0.2$ and $\theta = 10^\circ$.

4.5. Experimental tests and nonlinear geometric simulations

Following the analysis of the linear FE simulations, the next step is to examine the results obtained from the experimental tests on the additively-manufactured systems. In the figure 12, images of the undeformed and deformed structures upon being subjected to uniaxial tensile loading are shown, along with plots showing the results obtained from the DIC analysis of the images and the corresponding non-linear simulation runs. It is evident that in the cases of Structures 2 and 3 there is a very good match between the experimental results and the nonlinear FE simulations, while for Structure 1, the DIC data is rather noisy and indicates a Poisson's ratio which is slightly higher than that predicted by the nonlinear simulation. All systems show a *quasi*-linear strain-strain relationship with the Poisson's ratio remaining constant throughout the entire tensile loading strain range.

It is clear from the results obtained for Structure 3 (figure 12(c)), that this system exhibits auxetic behaviour as predicted by the FE simulations. The deformation profile observed during the experimental test also matches that indicated by the simulations. The same holds true for Structure 2, the SHT system, which exhibits a Poisson's ratio of zero that is maintained over a 7% strain range. In the case of Structure 1, on the other hand, some discrepancies can be observed between the experimental and FE simulations. The FE simulation underestimates the magnitude of the Poisson's ratio, predicting a value of +0.1, as opposed to the +0.3 obtained from the experimental test. This difference can be attributed to two factors. loss of length as a result of the overlap between ligaments at the interconnection region, is significantly First, the actual displacement used to induce 5% deformation is very small, hence the large amount of noise present in the DIC data points due to the relatively small deformation experienced by the central RUC. However, despite the lack of precision afford by the DIC readings, it is still clearly evident that the magnitude of the Poisson's ratio is higher than the predicted one. The second, and probably more significant reason, is the fact that unlike Structures 2 and 3, Structure 1 is characterised by honeycombs with a relatively small l/t ratio and thus, the effective length of these ligaments, when accounting for the reduced. This means that the predictions of the BEAM element simulations, which do not take into consideration the overlap of ligaments, will underestimate the magnitude of the Poisson's ratio, as well as the stiffness of the overall system. This effect has also been observed for auxetic re-entrant honeycombs

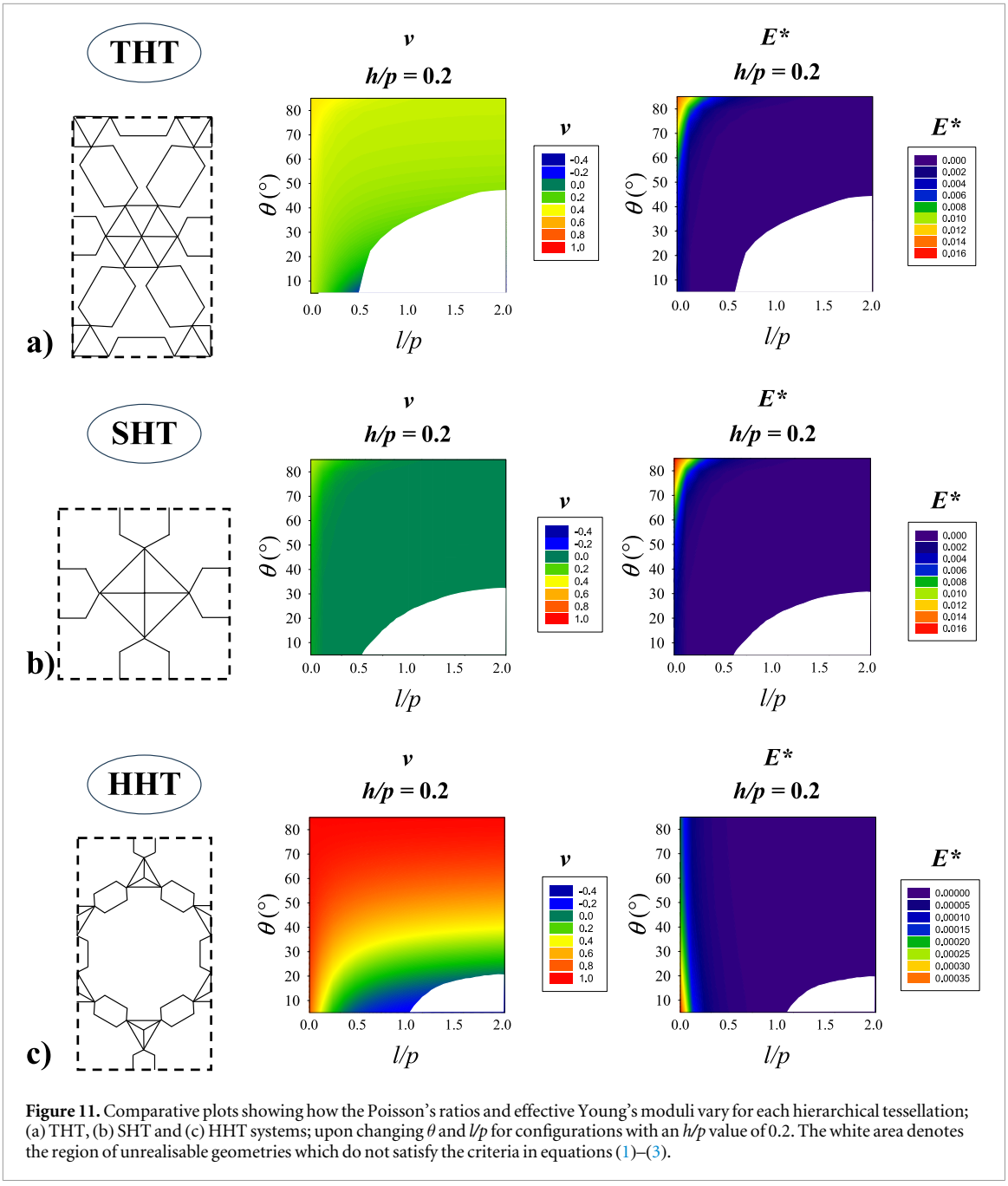

Figure 11. Comparative plots showing how the Poisson's ratios and effective Young's moduli vary for each hierarchical tessellation; (a) THT, (b) SHT and (c) HHT systems; upon changing θ and l/p for configurations with an h/p value of 0.2. The white area denotes the region of unrealisable geometries which do not satisfy the criteria in equations (1)–(3).

[10, 50, 51] where the influence of ligament overlap is more pronounced than in non re-entrant corresponding systems. This factor is not so important in the case where the ligaments are considerably slender, hence the reason why the correlation between simulations and experiments for the SHT and HHT systems is extremely good. Due to the strict geometric restriction for realizability of the THT systems (equation (1)), it is very difficult to design systems with small θ angles and large l values and thus, this discrepancy is expected to be present for the majority of THT systems. However, this does not mean that the FE results are inaccurate since the overall trends are still realistic and it merely indicates that the Poisson's ratio is slightly underestimated in magnitude for systems with relatively thick ligaments and one must take this factor into account.

4.6. General discussion and remarks

Before concluding, it is important to highlight the significance of this work and context in terms of the state-of-the-art. In this study we have introduced hierarchy in the three basic regular monohedral tilings; namely triangles, squares and hexagons; through the addition of strategically-placed irregular honeycombs. This geometric transformation has imparted significant versatility to these tessellatable networks in terms of allowing a wide range of permissible Poisson's ratios (including auxetic values which are not found in variants of the original tessellations) and Young's moduli whilst retaining their original symmetric framework. This

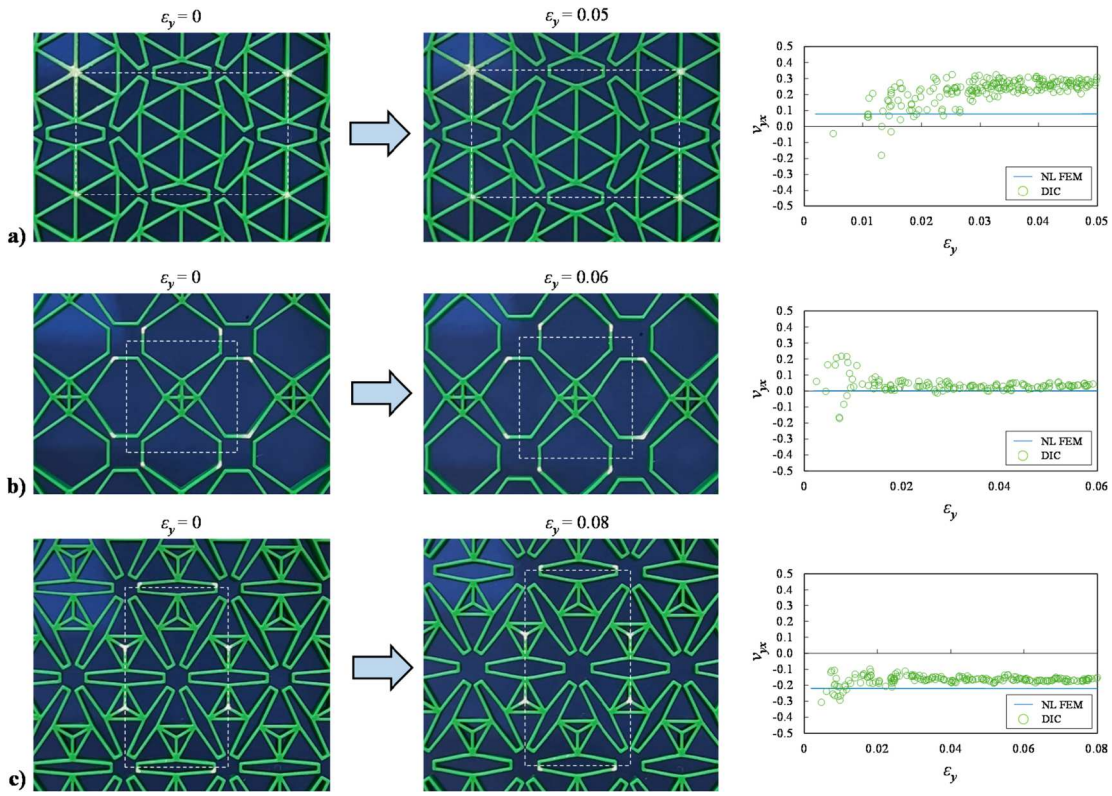

Figure 12. Comparison between experiments and FE simulations. The images show the deformation of the central RUC upon the application of a tensile load in the *y*-direction while the plots show the nonlinear FE simulation Poisson's ratio and the one obtained from the DIC analysis. The data points for the DIC were smoothened using the moving average method. Figure (a) shows Structure 1 (THT), (b) Structure 2 (SHT) and (c) Structure 3 (HHT).

latter point is extremely significant, since by retaining their symmetry, these tessellations also retain their original isotropic/orthotropic properties. In the case of THT and HHT systems, their hexagonal symmetry imparts transverse-isotropy, while for the SHT system, the orthotropy and on-axis equivalency of mechanical properties derived from their quadratic symmetry is retained. This means that the enhanced versatility afforded by the introduction of hierarchy does not come at a cost of symmetry breakage, and hence, anisotropy. Furthermore, the results obtained for the SHT and HHT systems are of particular interest. The former exhibits a *quasi*-constant Poisson's ratio of zero for the majority of configurations, while the Young's modulus varies significantly in comparison. This means that one can tailor the Young's modulus of this system independently of the Poisson's ratio which is extremely useful from a design perspective. The HHT system, on the other hand, is the system which shows the maximum versatility in terms of Poisson's ratio, with the FE simulations predicting values ranging from +1 to –0.24. For the most auxetic configurations, this change is particularly drastic, since the original monohedral regular hexagonal tessellation exhibits a Poisson's of +1 and highlights how effective the introduction of hierarchy can be in altering the mechanical properties and deformation mechanisms of these frameworks.

Future work on these systems can be focused on the high strain behaviour and energy absorption capabilities of these structures. Other advanced properties can also be incorporated into these systems through the use of smart constitutive materials such as shape memory materials to introduce shape morphing and programmable properties such as those implemented in other traditional metamaterial geometries [52–54]. We hope that this work acts as a foundation for further studies on the hierarchical geometric transformation of basic tessellations as well as more complex polyhedral networks involving honeycombs and other geometric features characteristic of auxetic systems and other mechanical metamaterials.

5. Conclusion

In this work a new class of hierarchical honeycomb-based mechanical metamaterials derived from triangular, square and hexagonal monohedral tessellations are presented. These systems were analysed through a wide-ranging parametric FE simulation run followed by experimental tests on three additively-manufactured prototypes. The introduction of hierarchy was shown to considerably enhance the versatility of these systems in

terms of permissible mechanical properties whilst retaining the original symmetry characteristics of the base tessellations. A select number of configurations were also shown to exhibit auxetic behaviour and zero Poisson's ratio; further demonstrating the profound influence which the hierarchical geometric structure has on the mechanical properties and deformation behaviour of these systems. The results obtained from the experimental tests showed good agreement with the FE simulations, demonstrating similar Poisson's ratios and deformation profiles. Given the wide range of mechanical properties afforded by these hierarchical tessellations, they may be utilised in various applications where mechanical metamaterials with tuneable mechanical characteristics are required.

Acknowledgments

This work was supported by the fondazione Cariplo and fondazione cdp grant no. 2023–2526 'support for young italian researchers in erc competitions' awarded to luke mizzi.

Data availability statement

All data that support the findings of this study are included within the article (and any supplementary files).

Author contributions

Michele Cavaliere
Methodology (lead), Formal analysis (lead), Investigation (lead), Validation (equal), Writing – original draft (lead)

Luke Mizzi 0000-0002-7650-1173
Conceptualization (lead), Supervision (lead), Validation (equal), Writing – review and editing (lead)

References

[1] Evans K E, Nkansah M A, Hutchinson I J and Rogers S C 1991 Molecular network design *Nature* **353** 124
[2] Zhang Y *et al* 2025 Recent advances of auxetic metamaterials in smart materials and structural systems *Adv. Funct. Mater.* 2421746
[3] Wojciechowski K W 1989 Two-dimensional isotropic system with a negative Poisson's ratio *Phys. Lett. A* **137** 60–4
[4] Wu W, Song X, Liang J, Xia R, Qian G and Fang D 2018 Mechanical properties of anti-tetrachiral auxetic stents *Compos. Struct.* **185** 381–92
[5] Bhullar S K 2013 Influence of negative poisson′s ratio on stent applications *Advances in Materials* **2** 42
[6] Ebrahimi M S, Noruzi M, Hamzehei R, Etemadi E and Hashemi R 2023 Revolutionary auxetic intravascular medical stents for angioplasty applications *Mater. Des.* **235** 112393
[7] Hasanzadeh R, Jolaiy S, Mojaver M, Azdast T and Park C B 2025 Auxetic 3D printed metastructure stents for enhanced mechanical and structural performance and biocompatibility in coronary artery treatments *Acta Biomater.* **202** 641–59
[8] Bezazi A and Scarpa F 2007 Mechanical behaviour of conventional and negative Poisson's ratio thermoplastic polyurethane foams under compressive cyclic loading *Int. J. Fatigue* **29** 922–30
[9] Mohsenizadeh S, Alipour R, Shokri Rad M, Farokhi Nejad A and Ahmad Z 2015 Crashworthiness assessment of auxetic foam-filled tube under quasi-static axial loading *Mater. Des.* **88** 258–68
[10] Masters I G and Evans K E 1996 Models for the elastic deformation of honeycombs *Compos. Struct.* **35** 403–22
[11] Evans K E, Alderson A and Christian F R 1995 Auxetic two-dimensional polymer networks an example of tailoring geometry for specific mechanical properties *J. Chem. Soc. Faraday Trans.* **91** 2671–80
[12] Shokri Rad M, Prawoto Y and Ahmad Z 2014 Analytical solution and finite element approach to the 3D re-entrant structures of auxetic materials *Mech. Mater.* **74** 76–87
[13] Grima J N, Gatt R, Alderson A and Evans K E 2005 On the potential of connected stars as auxetic systems *Mol. Simul.* **31** 925–35
[14] Grima J N and Evans K E 2000 Auxetic behavior from rotating squares *J. Mater. Sci. Lett.* **19** 1563–5
[15] Grima J N and Evans K E 2006 Auxetic behavior from rotating triangles *J. Mater. Sci.* **41** 3193–6
[16] Alderson A *et al* 2010 Elastic constants of 3-, 4- and 6-connected chiral and anti-chiral honeycombs subject to uniaxial in-plane loading *Compos. Sci. Technol.* **70** 1042–8
[17] Mizzi L and Spaggiari A 2021 Chiralisation of euclidean polygonal tessellations for the design of new auxetic metamaterials *Mech. Mater.* **153** 103698
[18] Prall D and Lakes R S 1997 Properties of a chiral honeycomb with a poisson's ratio of -1 *Int. J. Mech. Sci.* **39** 305–14
[19] Caporale A M, Airoldi A and Novak N 2024 A novel body centered cubic 3D auxetic chiral geometry *Smart Mater. Struct.* **34** 015050
[20] Silverberg J L *et al* 2014 Using origami design principles to fold reprogrammable mechanical metamaterials *Science* **345** 647–9
[21] Schenk M and Guest S D 2013 Geometry of miura-folded metamaterials *Proc. Natl. Acad. Sci. U S A* **110** 3276–81
[22] Gatt R *et al* 2015 Hierarchical auxetic mechanical metamaterials *Sci. Rep.* **5** 8395
[23] Lakes R S 1993 Materials with structural hierarchy *Nature* **361** 511–5
[24] Ajdari A, Jahromi B H, Papadopoulos J, Nayeb-Hashemi H and Vaziri A 2012 Hierarchical honeycombs with tailorable properties *Int. J. Solids Struct.* **49** 1413–9

[25] Kunin V, Yang S, Cho Y, Deymier P and Srolovitz D J 2016 Static and dynamic elastic properties of fractal-cut materials *Extreme Mech. Lett.* **6** 103–14
[26] Cho Y *et al* 2014 Engineering the shape and structure of materials by fractal cut *Proc. Natl. Acad. Sci. U S A* **111** 17390–5
[27] Meza L R, Zelhofer A J, Clarke N, Mateos A J, Kochmann D M and Greer J 2015 Resilient 3D hierarchical architected metamaterials *Proc. Natl. Acad. Sci. U S A* **112** 11502–7
[28] Rayneau-Kirkhope D 2018 Stiff auxetics: hierarchy as a route to stiff, strong lattice based auxetic meta-materials *Sci. Rep.* **8** 12437
[29] Mizzi L and Spaggiari A 2020 Lightweight mechanical metamaterials designed using hierarchical truss elements *Smart Mater. Struct.* **29** 105036
[30] Mizzi L, Dudek K K, Frasinetti A, Spaggiari A, Ulliac G and Kadic M 2025 Lightweight 3d hierarchical metamaterial microlattices *Adv. Sci.* **34** 2110115
[31] Tang Y, Lin G, Han L, Qiu S, Yang S and Yin J 2015 Design of hierarchically cut hinges for highly stretchable and reconfigurable metamaterials with enhanced strength *Adv. Mater.* **27** 7181–90
[32] Wu W *et al* 2017 Mechanical properties of hierarchical anti-tetrachiral metastructures *Extreme Mech. Lett.* **16** 18–32
[33] Dudek K K, Martínez J A I, Ulliac G and Kadic M 2022 Micro-scale auxetic hierarchical mechanical metamaterials for shape morphing *Adv. Mater.* **34** 18–32
[34] Yang H, Wang B and Ma L 2019 Designing hierarchical metamaterials by topology analysis with tailored Poisson's ratio and Young's modulus *Compos. Struct.* **214** 359–78
[35] Mousanezhad D, Haghpanah B, Ghosh R, Hamouda A M, Nayeb-Hashemi H and Vaziri A 2016 Elastic properties of chiral, anti-chiral, and hierarchical honeycombs: a simple energy-based approach *Theoretical and Applied Mechanics Letters* **6** 81–96
[36] Attard D, Farrugia P S, Gatt R and Grima J N 2020 Starchirals–a novel class of auxetic hierarchal structures *Int. J. Mech. Sci.* **179** 105631
[37] Mousanezhad D *et al* 2016 Hierarchical honeycomb auxetic metamaterials *Sci. Rep.* **5** 18306
[38] Dudek K K *et al* 2017 On the dynamics and control of mechanical properties of hierarchical rotating rigid unit auxetics *Sci. Rep.* **7** 46529
[39] Gao E, Li R, Fang S, Shao Q and Baughman R H 2021 Bounds on the in-plane poisson's ratios and the in-plane linear and area compressibilities for sheet crystals *J. Mech. Phys. Solids* **152** 104409
[40] Ting T C T and Chen T 2005 Poisson's ratio for anisotropic elastic materials can have no bounds *Q. J. Mech. Appl. Math.* **58** 73–82
[41] Mizzi L, Attard D, Gatt R, Dudek K K, Ellul B and Grima J N 2021 Implementation of periodic boundary conditions for loading of mechanical metamaterials and other complex geometric microstructures using finite element analysis *Eng. Comput.* **37** 1765–79
[42] Moghimimonfared R, Spaggiari A, Grasselli L and Mizzi L 2025 Hexagonal tessellation-based mechanical metamaterials *Extreme Mech. Lett.* **77** 102356
[43] Mizzi L, Salvati E, Spaggiari A, Tan J C and Korsunsky A M 2020 Highly stretchable two-dimensional auxetic metamaterial sheets fabricated via direct-laser cutting *Int. J. Mech. Sci.* **167** 105242
[44] Gibson L J, Ashby M F, Schajer G S and Robertson C I 1982 The mechanics of two dimensional cellular materials *Proc. R. Soc.* A **382** 25–42
[45] Olympio K R and Gandhi F 2010 Zero poisson's ratio cellular honeycombs for flex skins undergoing one-dimensional morphing *J. Intell. Mater. Syst. Struct.* **21** 1737–53
[46] Grima J N *et al* 2010 Hexagonal honeycombs with zero poisson's ratios and enhanced stiffness *Adv. Eng. Mater.* **12** 855–62
[47] Attard D and Grima J N 2011 Modelling of hexagonal honeycombs exhibiting zero Poisson's ratio *Phys. Status Solidi* B **248** 52–9
[48] Ashby M F 2005 The properties of foams and lattices *Proc. R. Soc.* A **364** 15–30
[49] Fowler P W and Guest S D 2000 A symmetry extension of maxwell's rule for rigidity of frames *Int. J. Solids Struct.* **37** 1793–804
[50] Balawi S and Abot J L 2008 A refined model for the effective in-plane elastic moduli of hexagonal honeycombs *Compos. Struct.* **84** 147–58
[51] Mizzi L, Attard D, Casha A, Grima J N and Gatt R 2014 On the suitability of hexagonal honeycombs as stent geometries *Phys. Status Solidi.* B **251** 328–37
[52] Dong Y, Chen K, Liu H, Li J, Liang Z and Kan Q 2024 Adjustable mechanical performances of 4D-printed shape memory lattice structures *Compos. Struct.* **334** 117971
[53] Li J, Zhong W, Xu J, Wang X, Chen J and Li J 2025 An elongation-shortening strategy modifying the deformation mechanism of cellular structure for excellent energy absorption *Virtual Phys Prototyp.* **20** e2503259
[54] Dudek K K, Kadic M, Coulais C and Bertoldi K 2025 Shape-morphing metamaterials *Nat. Rev. Mater.* (https://doi.org/10.1038/s41578-025-00828-9)